MITSUBISHI ELECTRIC RESEARCH LABORATORIES
https://www.merl.com

# Extremum Seeking-Based Observer Design for Reduced Order Models of Coupled Thermal and Fluid Systems

Koga, Shumon; Benosman, Mouhacine; Borggaard, Jeff

TR2021-065 June 04, 2021

**Abstract**

We present an extremum seeking-based robust observer design for thermal-fluid systems, pursuing an application to efficient energy management in buildings. The model is originally described by Boussinesq equations which is given by a system of two coupled partial differential equations (PDEs) for the velocity field and temperature profile constrained to incompressible flow. Using proper orthogonal decomposition (POD), the PDEs are reduced to a set of nonlinear ordinary differential equations (ODEs). Given a set of temperature and velocity point measurements, a nonlinear state observer is designed to reconstruct the entire state under the error of initial states, and model parametric uncertainties. We prove that the closed loop system for the observer error state satisfies an estimate of L2 norm in a sense of locally input-tostate stability (LISS) with respect to parameter uncertainties. Moreover, the uncertain parameters estimate used in the designed observer are optimized through iterations of a data-driven extremum seeking (ES) algorithm. Numerical simulation of a 2D Boussinesq PDE illustrates the performance of the proposed adaptive estimation method.

*International Journal of Adaptive Control and Signal Processing*



Mitsubishi Electric Research Laboratories, Inc.
201 Broadway, Cambridge, Massachusetts 02139

INTERNATIONAL JOURNAL OF ADAPTIVE CONTROL AND SIGNAL PROCESSING
*Int. J. Adapt. Control Signal Process.* 2019; **00**:1–26
Published online in Wiley InterScience (www.interscience.wiley.com). DOI: 10.1002/acs

# Extremum Seeking-Based Observer Design for Reduced Order Models of Coupled Thermal and Fluid Systems

Shumon Koga, Mouhacine Benosman* , Jeff Borggaard

*S. Koga, intern at MERL, is with the Department of Mechanical and Aerospace Engineering, U.C. San Diego, 9500 Gilman Drive, La Jolla, CA, 92093-0411. M. Benosman is with Mitsubishi Electric Research Laboratories (MERL), Cambridge, MA, 02139. J. Borggaard is with the Interdisciplinary Center for Applied Mathematics, Virginia Tech, Blacksburg, VA, 24061*

SUMMARY

We present an extremum seeking-based robust observer design for thermal-fluid systems, pursuing an application to efficient energy management in buildings. The model is originally described by Boussinesq equations which is given by a system of two coupled partial differential equations (PDEs) for the velocity field and temperature profile constrained to incompressible flow. Using proper orthogonal decomposition (POD), the PDEs are reduced to a set of nonlinear ordinary differential equations (ODEs). Given a set of temperature and velocity point measurements, a nonlinear state observer is designed to reconstruct the entire state under the error of initial states, and model parametric uncertainties. We prove that the closed loop system for the observer error state satisfies an estimate of $L_2$ norm in a sense of locally input-to-state stability (LISS) with respect to parameter uncertainties. Moreover, the uncertain parameters estimate used in the designed observer are optimized through iterations of a data-driven extremum seeking (ES) algorithm. Numerical simulation of a 2D Boussinesq PDE illustrates the performance of the proposed adaptive estimation method. Copyright © 2019 John Wiley & Sons, Ltd.

Received . . .

KEY WORDS: Extremum seeking, iterative feedback tuning, thermo-fluid models, observer design, input-state stability, Boussinesq equation.

## 1. INTRODUCTION

Thermal and fluid systems have been intensively studied for numerous applications in science and engineering processes. For instance, an efficient energy management for heating, ventilation, and

*Corresponding author:m_benosman@ieee.org

air conditioning (HVAC) systems has been a priority research topic for many countries due to its huge energy consumption impact [6].

One of the important problems in HVAC management is to estimate the entire spatial profile of the airflow and temperature under a limited number of sensors placed at some locations in buildings. Such a state estimation for Navier Stokes (NS) equations has been investigated in a number of literatures in the recent decade. In [8], an infinite dimensional Kalman filter is designed for a linearized NS equation around the velocity field of interest. Their approach showed good performance as a first contribution to fluid estimation, however, there are two issues from the perspective of real implementation. One is the linearization assumption of NS equations, can produce a low fidelity fluid model. A second drawback is the high computational cost for the discretization of the infinite dimensional filter. To improve these issues, in [11], the authors developed a POD-based model reduction for NS equations, and designed extended Kalman filter for the state estimation, which illustrated the effective results on estimated velocity profile. The later work on state estimation for POD-ROM of NS equations can be found in [12, 15].

For higher fidelity models of the NS equation which include the effect of buoyancy forces driven by the density change via temperature dependence. The dynamics of the temperature profile is also described from the conservation of energy, which formulates the Boussinesq equations as a coupled thermal and fluid systems. Due to the coupled nonlinearity of two PDEs, the design and analysis of Boussinesq equations is highly challenging problem especially for 2D and 3D domains. Moreover, as presented in [13], POD-based model reduction might lose the stability property of the state variables, which is caused by the truncation of higher order modes serving as a stabilizing factor. While there are several methods for model reduction, the modal analysis has been successfully employed for PDEs with state constraints in [10, 23].

The stable model reduction for Boussinesq equations is developed in [4] by introducing a new closure model, which robustly stabilizes the reduced order model. The authors prove the robust stability of the closure model with respect to the parameters uncertainty using Lyapunov analysis. Furthermore, the gains in the closure terms are auto-tuned by learning-based extremum seeking (ES) algorithm to minimize the errors between the true model solution and the ROM solution. The convergence analysis of ES is established in [14] by means of singular perturbation and averaging theorem, and an approach to apply ES for parameter auto-tuning in POD-ROM is originated in [5]. The results in [4] illustrate a good performance in improving solution prediction for laminar flows, however, the method relies on the accurate knowledge of the initial velocity and temperature profiles, which can be relaxed by state estimation technique utilizing sparse measurements obtained through a few sensors.

There are two contributions in this paper. First, we have investigated the robustness of the designed observer for POD-ROM of Boussinesq equation with respect to the uncertainty of viscosity




DOI: 10.1002/acs

by proving input-to-state stability (ISS) in a local sense using Lyapunov method. The observer gain is designed via LMI approach to satisfy a condition for ISS proof. Second, as in [4], the online estimation of the uncertain viscosity parameter is implemented using a data-driven extremum seeking.

This paper is structured as follows. In Section 3, the physical model of thermal and fluid systems is introduced by means of Boussinesq equations, and its POD-ROM is derived. Section 4 is devoted to the observer design for POD-ROM, where we provide the robustness analysis with respect to parameter uncertainty. In Section 5, the online estimation of the uncertain parameter in the designed observer is performed by ES as an iterative learning estimation, and Section 6 presents the numerical verification of the proposed method for 2-D Boussinesq equations. The paper ends with a conclusion and future works, as stated in Section 7.

## 2. PRELIMINARY DEFINITIONS

Throughout the paper, we use $\|\cdot\|$ to denote the Euclidean norm; i.e., for a vector $x \in \mathbb{R}^n$, we have $\|x\| \triangleq \|x\|_2 = \sqrt{x^T x}$, where $x^T$ denotes the transpose of the vector $x$. The Frobenius norm of a matrix $A \in \mathbb{R}^{m\times n}$, with elements $a_{ij}$, is defined as $\|A\|_F \triangleq \sqrt{\sum_{i=1}^{n}\sum_{j=1}^{n}|a_{ij}|^2}$. Given $x \in \mathbb{R}^m$. We use $\dot{f}$ to denote the time derivative of $f$ and $f^{(r)}(t)$ for the $r$-th derivative of $f(t)$, i.e., $f^{(r)} \triangleq \frac{d^r f}{dt^r}$. We denote by $\mathbb{C}^k$, functions that are $k$ times differentiable and by $\mathbb{C}^\infty$, a smooth function. A continuous function $\alpha : [0, a) \to [0, \infty)$ is said to belong to class $\mathcal{K}$ if it is strictly increasing and $\alpha(0) = 0$. It is said to belong to class $\mathcal{K}_\infty$ if $a = \infty$ and $\alpha(r) \to \infty$ as $r \to \infty$ [1]. A continuous function $\beta : [0, a) \times [0, \infty) \to [0, \infty)$ is said to belong to class $\mathcal{KL}$ if, for a fixed $s$, the mapping $\beta(r, s)$ belongs to class $\mathcal{K}$ with respect to $r$ and, for each fixed $r$, the mapping $\beta(r, s)$ is decreasing with respect to $s$ and $\beta(r, s) \to 0$ as $s \to \infty$ [1]. Finally, for a Hilbert space $\mathcal{H}$, we define the inner product $\langle\cdot,\cdot\rangle_{\mathcal{H}}$ and the associated norm $\|\cdot\|_{\mathcal{H}}$ on $\mathcal{H}$ as $\langle f, g\rangle_{\mathcal{H}} = \int_\Omega f(x)g(x)dx$, for $f, g \in \mathcal{H}$, and $\|f\|^2_{\mathcal{H}} = \int_\Omega |f(x)|^2 dx$

Next, we introduce some definitions that will be used in the sequel, e.g. [1]: consider the system

$$\dot{x} \;=\; f(t, x, u), \tag{1}$$

where $f : [0, \infty) \times \mathbb{R}^n \times \mathbb{R}^m \to \mathbb{R}^n$ is piecewise continuous in $t$ and locally Lipschitz in $x$ and $u$, uniformly in $t$. The input $u(t)$ is piecewise continuous, bounded function of $t$ for all $t \geq 0$.

*Definition 1* ([1, 2])
The system (1) is said to be *input-to-sate stable* (ISS) if there exist a class $\mathcal{KL}$ function $\beta$ and a class $\mathcal{K}$ function $\gamma$ such that for any initial state $x(t_0)$ and any bounded input $u(t)$, the solution $x(t)$ exists




DOI: 10.1002/acs

for all $t \geq t_0$ and satisfies

$$\|x(t)\| \leq \beta(\|x(t_0)\|, t - t_0) + \gamma(\sup_{t_0 \leq \tau \leq t} \|u(\tau)\|).$$

*Theorem 1* ([1, 2])
Let $V : [0, \infty) \times \mathbb{R}^n \to \mathbb{R}$ be a continuously differentiable function such that

$$\begin{aligned} \alpha_1(\|x\|) \leq & V(t, x) \leq \alpha_2(\|x\|), \\ \frac{\partial V}{\partial t} + \frac{\partial V}{\partial x} f(t, x, u) \leq & -W(x), \quad \forall \|x\| \geq \rho(\|u\|) > 0, \end{aligned} \tag{2}$$

for all $(t, x, u) \in [0, \infty) \times \mathbb{R}^n \times \mathbb{R}^m$, where $\alpha_1$, $\alpha_2$ are class $\mathcal{K}_\infty$ functions, $\rho$ is a class $\mathcal{K}$ function, and $W(x)$ is a continuous positive definite function on $\mathbb{R}^n$. Then, the system (1) is input-to-state stable (ISS).

## 3. MODELLING OF THERMAL AND FLUID SYSTEMS

### *3.1. Boussinesq equations and normalization*

We focus on the dynamics of the velocity field $\boldsymbol{v}(x, t) : \Omega \times \mathbb{R}^+ \to \mathbb{R}^3$ and the temperature profile $T(x, t) : \Omega \times \mathbb{R}^+ \to \mathbb{R}$, where $x$ denotes the spatial coordinate $x \in \Omega$, and $t \geq 0$ denotes the time. The spatial domain $\Omega$ can be two or three dimensional space. The governing equations are described by Navier-Stokes equation with the condition of incompressible flow and the conservation of the energy through the heat transfer, which leads to the following coupled system

$$\rho \left( \frac{\partial \boldsymbol{v}}{\partial t} + \boldsymbol{v} \cdot \nabla \boldsymbol{v} \right) = - \nabla p + \nabla \cdot \tau(\boldsymbol{v}) + \rho \boldsymbol{g}, \tag{3}$$

$$\nabla \cdot \boldsymbol{v} = 0, \tag{4}$$

$$\rho c_p \left( \frac{\partial T}{\partial t} + \boldsymbol{v} \cdot \nabla T \right) = \nabla \left( \kappa \nabla T \right), \tag{5}$$

where $\rho$ $[kg/m^3]$ is the density profile, $p$ $[kg/(ms^2)]$ is the pressure field, $\tau(\boldsymbol{v})$ is the viscous stress, $c_p$ $[J/kg^\circ K]$ is the constant heat capacity, $\kappa$ $[W/m^\circ K]$ is the constant thermal conductivity, and $\boldsymbol{g} = -g\boldsymbol{e}_3$ $[m/s^2]$ is the gravitational force. In Boussinesq approximation, the buoyancy force is driven by changes in density $\rho = \rho_0 + \Delta\rho$ from the nominal density $\rho_0$, and the density change is modeled as perturbations from the nominal temperature $T_0$ using the perfect gas law $\Delta\rho\boldsymbol{g} = -\rho_0\beta(T - T_0)\boldsymbol{g}$, $\beta = 1/T_0$, and the constant term $\rho_0\boldsymbol{g}$ is absorbed into the pressure. The viscous stress is governed by $\tau(\boldsymbol{v}) = \rho\nu(\nabla\boldsymbol{v} + \nabla\boldsymbol{v}^T)$ with kinematic viscosity $\nu$ $[m^2/s]$, whereas the velocity $\boldsymbol{v}$ is in $[m/s]$, and the temperature $T$ is in $[K]$.



*Prepared using* acsauth.cls
DOI: 10.1002/acs

By introducing a characteristic length $L$, characteristic velocity $\boldsymbol{v}_0$, wall temperature $T_w$, we define the following normalized states

$$\tilde{x} = \frac{x}{L}, \quad \tilde{t} = \frac{t\boldsymbol{v}_0}{L}, \quad \tilde{v} = \frac{v}{v_0}, \tag{6}$$

$$\tilde{p} = \frac{p}{\rho v_0^2}, \quad \tilde{T} = \frac{T - T_0}{T_w - T_0}. \tag{7}$$

Using these variables, PDEs (3)–(5) can be reduced to the following (we dropped the tilde notation)

$$\frac{\partial \boldsymbol{v}}{\partial t} + \boldsymbol{v} \cdot \nabla \boldsymbol{v} = -\nabla p + \nabla \cdot \tau(\boldsymbol{v}) + \frac{\mathrm{Gr}}{\mathrm{Re}^2} T \boldsymbol{e}_3, \tag{8}$$

$$\nabla \cdot \boldsymbol{v} = 0, \tag{9}$$

$$\frac{\partial T}{\partial t} + \boldsymbol{v} \cdot \nabla T = \nabla \left( \frac{1}{\mathrm{RePr}} \nabla T \right), \tag{10}$$

where we defined Reynolds number $\mathrm{Re} = \frac{v_0 L}{\nu}$, Grashof number $\mathrm{Gr} = \frac{g\beta(T_w - T_0)L^3}{\nu^2}$, and Prandtl number $\mathrm{Pr} = \frac{nu}{k/\rho_0 c_p}$.

### *3.2. POD Model Reduction*

Following Galerkin projection onto the subspace spanned by the POD basis functions, we have

$$\boldsymbol{v}^{pod}(x,t) = \boldsymbol{v}_0(x) + \sum_{i=1}^{r_v} q_i(t) \phi_i^{\boldsymbol{v}}(x), \tag{11}$$

$$T^{pod}(x,t) = T_0(x) + \sum_{i=r_{\boldsymbol{v}}+1}^{r_{\boldsymbol{v}}+r_T} q_i(t) \phi_i^{T}(x), \tag{12}$$

where $\boldsymbol{v}_0(x)$ and $T_0(x)$ are the steady-state solution to (3)–(5), $\phi_i^{\boldsymbol{v}}(x)$ and $\phi_i^T(x)$ are POD basis functions given by

$$\phi_i^{\boldsymbol{v}}(x) = \frac{1}{t_f} \int_0^{t_f} (\boldsymbol{v}_{sim}(x,t) - \boldsymbol{v}_0(x)) w_i(t) dt, \tag{13}$$

for $i = 1, \cdots, r_{\boldsymbol{v}}$, and

$$\phi_i^{T}(x) = \frac{1}{t_f} \int_0^{t_f} (T_{sim}(x,t) - T_0(x)) w_i(t) dt, \tag{14}$$

for $i = r_{\boldsymbol{v}} + 1, \cdots, r_{\boldsymbol{v}} + r_T$, with the orthogonal wight functions $w_i(t)$ satisfying $\int_0^{t_f} w_i(t) w_j(t) dt = 0$ if $i \neq j$. The coefficients $q_i(t)$ in (11) and (12) are the dynamical states representing the POD-ROM of the Boussinesq equations.

*Remark 1*

**POD-projection error, e.g., [24]:** Let $\mathcal{T} : \mathcal{H} \to \hat{\mathcal{H}}$ be the orthogonal projector from $\mathcal{H}$ (infinite dimension Hilbert space) to the finite dimension space $\hat{\mathcal{H}}$ (hence, $\|\mathcal{T}\|_{\mathcal{H}} = 1$ and $\mathcal{T}^\dagger$ be the injection from $\hat{\mathcal{H}}$ into $\mathcal{H}$: $\mathcal{T}^\dagger \hat{z} = z$ for all $\hat{z} \in \hat{\mathcal{H}} \subset \mathcal{H}$. Then we define the *reduced estimation error* as

$$e(t) = \hat{z}(t) - \mathcal{T} z(t) \in \hat{\mathcal{H}}. \tag{15}$$




DOI: 10.1002/acs

This can be used as a proxy for the *state estimation error*

$$e_{\rm se} \equiv \mathcal{T}^\dagger \hat{z} - z \in \mathcal{H}, \tag{16}$$

when $\mathcal{T}$ produces a small projection error $(z - \mathcal{T}^\dagger \mathcal{T} z)$, since

$$e_{\rm se}(t) = \mathcal{T}^\dagger e(t) - \left(z(t) - \mathcal{T}^\dagger \mathcal{T} z(t)\right). \tag{17}$$

When $\hat{\mathcal{H}}$ is the span of $r$ dominant POD basis functions and $\mathcal{T}_{\rm POD}$ is the corresponding projection for a specific trajectory $z$, i.e., $\mathcal{T} \equiv \mathcal{T}_{\rm POD} : \mathcal{H} \to \hat{\mathcal{H}}_r$ as follows

$$\left[\mathcal{T}_{\rm POD} z\right](\cdot) = \sum_{i=1}^{r} \phi_i(\cdot) \langle \phi_i, z \rangle_{\mathcal{H}}. \tag{18}$$

then $\mathcal{T}_{\rm POD}$ minimizes the projection error

$$\mathcal{P}(\mathcal{T}, z) = \left( \int_0^{t_f} \| z(t) - \mathcal{T}^\dagger \mathcal{T} z(t) \|_{\mathcal{H}}^2 \, dt \right)^{1/2}, \tag{19}$$

over all projections $\mathcal{T}$ into subspaces of $\mathcal{H}$ with dimension $r$, and where $t_f$ denotes the finite time support over which the projection error is evaluated, cf. [25].

By defining the state vector $q(t) = [q_1(t), q_2(t), \cdots, q_{r_v + r_T}(t)]^T$, we obtain the following ODE (see [4] for the detailed derivation)

$$\dot{q}(t) = \mu D q(t) + [C q(t)] q(t) + b, \tag{20}$$

where $\mu > 0$ is the viscosity $\mu = \frac{1}{\rm Re}$, $D$ is a negative definite diffusion matrix with diagonal blocks corresponding to the viscous stress and thermal diffusion, and $C$ is a three-dimensional tensor corresponding the convection terms in (8) and (10). In the remaining of this paper, we shall call the model (20) as ROM-G (G for Galerkin).

*Remark 2*

While the original PDEs (3)–(5) is a system that has bounded solutions from our knowledge on thermal and fluid dynamics, the obtained POD-ROM (20) might exhibits radially unbounded solutions depending on the strength of the quadratic nonlinearity $[Cq(t)]q(t)$ and the constant term $b$ relative to the damping effect $\mu D q(t)$. We study the effect of $\mu$ on the boundedness of the solution to (20) in the next lemma.

*Lemma 1*

For a viscosity coefficient satisfying

$$\mu \geq \frac{2}{\underline{d}} \max\left\{ \sqrt{c_{\max} b_{\max}}, c_{\max} ||q_0|| \right\}, \tag{21}$$

where $\underline{d} := \lambda_{\min}(-D) > 0$, $c_{\max} = ||C||_F$, $b_{\max} = ||b||$, the following explicit bound holds

$$||q|| \leq Y^* + \frac{\bar{b}}{c_{\max} + \left( \frac{\bar{b}}{||q_0|| - Y^*} - c_{\max} \right) e^{\bar{b} t}}, \tag{22}$$



*Prepared using* acsauth.cls
DOI: 10.1002/acs

where $\bar{b} = \sqrt{\mu^2 \underline{d}^2 - 4 b_{\max} c_{\max}}$, and $Y^* = \frac{\mu \underline{d} - \bar{b}}{2 c_{\max}}$. Moreover, the solution is uniformly bounded by a positive constant $M = \frac{\mu \underline{d}}{2 c_{\max}}$, i.e., $||q|| \leq M$.

*Proof*

Consider the following Lyapunov function

$$V = q^T q = ||q||^2. \tag{23}$$

Taking the time derivative of (23) and using (20) yields

$$\dot{V} = \mu q^T (D + D^T) q + 2[Cq] q^T q + 2 b^T q. \tag{24}$$

Due to the negative definiteness of $D = D^T < 0$, we have

$$q^T (D + D^T) q \leq -2 \underline{d} ||q||^2. \tag{25}$$

By the Cauchy Schwarz inequality, it holds that

$$[Cq] q^T q \leq c_{\max} ||q||^3, \quad b^T q \leq b_{\max} ||q||. \tag{26}$$

Applying (25) and (26) to (24), one can derive the following differential inequality

$$\dot{V} \leq -2 \mu \underline{d} ||q||^2 + 2 c_{\max} ||q||^3 + 2 b_{\max} ||q||. \tag{27}$$

Next, we consider

$$Y = \sqrt{V} = ||q||. \tag{28}$$

Then, the time derivative of (28) is

$$\begin{aligned} \dot{Y} =& \frac{\dot{V}}{2Y} \\ \leq& -\mu \underline{d} Y + c_{\max} Y^2 + b_{\max} \end{aligned} \tag{29}$$

Applying comparison principle to (29), $Y$ is bounded by the solution to the Riccati differential equation $\dot{y} = -\mu \underline{d} y + c_{\max} y^2 + b_{\max}$ with initial condition $y(0) = Y(0)$. If the viscosity is sufficiently large to satisfy (21), the solution of $y(t)$ is given by the right hand side of (22). Hence, $Y$ satisfies the inequality (22). Moreover, by condition (21), we have $||q_0|| \leq \frac{\mu \underline{d}}{2 c_{\max}}$. Applying this to (22), the bound $||q|| \leq Y^* + \frac{\bar{b}}{c_{\max}(1 + e^{\bar{b} t})}$ is obtained. Since $\frac{\bar{b}}{c_{\max}(1 + e^{\bar{b} t})} \leq \frac{\bar{b}}{2 c_{\max}}$ and $Y^* = \frac{\mu \underline{d} - \bar{b}}{2 c_{\max}}$, the uniform bound $||q|| \leq \frac{\mu \underline{d}}{2 c_{\max}}$ is deduced. □

### *3.3. Closure model for ROM stabilization*

The main idea behind the closure modeling is to replace the viscosity coefficient $\mu$ in (20) by a virtual viscosity coefficient $\mu_{\mathrm{cl}}$, which is chosen to stabilize the POD-ROM. Furthermore, a penalty




DOI: 10.1002/acs

term $H(q(t))$ is added to the POD-ROM as follows

$$\dot{q}(t) = \mu_{\rm cl} D q(t) + \tilde{F}(q) + H(q(t)), \tag{30}$$

where $\tilde{F}(q)$ is defined as

$$\tilde{F}(q) = [Cq(t)]q(t) + b. \tag{31}$$

A well known choice of the virtual viscosity is the Heisenberg ROM (ROM-H) which is simply given by

$$\mu_{\rm cl} = \mu_0 + \mu_e, \tag{32}$$

where $\mu_0$ is the nominal value of the viscosity coefficient, and $\mu_e$ is the additional constant added to compensate for the loss of the damping effect of the truncated modes. The choice of $H(q)$ is presented in [4] based on the function of $\tilde{F}(q)$, by imposing the following assumption.

*Assumption 1*
There exists a $\mathcal{C}_1$ function $\tilde{f}(q) : \mathbb{R}^n \to \mathbb{R}$ such that the norm of vector field $\tilde{F}(q) : \mathbb{R}^n \to \mathbb{R}^n$ is bounded, i.e.,

$$||\tilde{F}(q)|| \leq \tilde{f}(q). \tag{33}$$

Using the vector field function (31), the bounded function $\tilde{f}$ is given by

$$\tilde{f}(q) = c_{\max}||q||^2 + b_{\max}, \tag{34}$$

where $c_{\max} = ||C||_F$, and $b_{\max} = ||b||_{L_\infty}$. In [4], the authors proved the following lemma.

*Lemma 2*
Let Assumption 1 holds. Then, the reduced order model (30) with

$$H(q) = \mu_{\rm nl} \tilde{f}(q) D^* q, \quad \mu_{\rm nl} > 0 \tag{35}$$

where $D^* = \mathrm{diag}(d_{11}, d_{22}, \cdots, d_{rr})$, stabilizes the solution of the ROM to the invariant set

$$\mathcal{S} = \left\{ q \in \mathbb{R}^n \quad \text{s.t.} \quad \mu_{\rm cl} \frac{\lambda_{\max}(D)||q||}{\tilde{f}(q)} + \mu_{\rm nl}||q|| \max\{d_{11}, \cdots, d_{rr}\} + 1 \geq 0 \right\}. \tag{36}$$

Thus, the nonlinear reduced order model with closure model $H$ is given by

$$\dot{q}(t) = \mu_{\rm cl} D q(t) + [Cq(t)]q(t) + b + \mu_{\rm nl}(c_{\max}||q||^2 + b_{\max}) D^* q. \tag{37}$$

In the remaining of this paper, we shall call the model (37) as ROM-CL (CL stands for closure).



*Prepared using* acsauth.cls
DOI: 10.1002/acs

## 4. ROBUSTNESS OF NONLINEAR OBSERVER IN LOCAL ISS SENSE

### *4.1. Observer based on the ROM-G model*

To solve for the POD-ROM in (20), the values of the viscosity parameter $\mu_{\text{cl}}$ and the initial conditions $q(0)$ are needed, however, in most applications they are uncertain. Instead, we can allocate thermal and velocity sensors to measure some partial states of the system, which can be formulated as a linear map from the POD states

$$y(t) = \tilde{H}q(t), \tag{38}$$

where $\tilde{H} \in \mathbb{R}^{m\times n}$ is a measurement matrix given by the sensor placement. Then, to assimilate the model (20) with the acquired sensor data, the state estimator is designed to reconstruct the entire state $q(t)$ from the measured data, which enables to estimate the velocity field $\boldsymbol{v}^{pod}(x,t)$ and the temperature profile $T^{pod}(x,t)$ for all $x$. A well-known design is Luenberger-like observer which is constructed as a copy of the plant plus the injection of the measurement error states, written by

$$\dot{\hat{q}}(t) = \hat{\mu}_{\text{cl}} D\hat{q}(t) + [C\hat{q}(t)]\hat{q}(t) + b + L(y(t) - \tilde{H}\hat{q}(t)), \tag{39}$$

where $\hat{q}(t)$ is the estimation of states $q(t)$, $\hat{\mu}_{\text{cl}}$ is the estimated value of $\mu_{\text{cl}}$, and $L \in \mathbb{R}^{n\times m}$ is the observer gain to be determined. For analysis purposes, we impose the following assumption.

*Assumption 2*

The lower bound of the viscosity $\mu_{\text{cl}}$ is known, i.e., $\underline{\mu} \leq \mu_{\text{cl}}$. Furthermore, our estimated value of the viscosity also satisfies $\underline{\mu} \leq \hat{\mu}_{\text{cl}}$.

Let $\tilde{q}(t)$ be the estimation error state defined by

$$\tilde{q}(t) := q(t) - \hat{q}(t). \tag{40}$$

The ideal performance of the observer is characterized by some sort of the stability property of the estimation error $\tilde{q}(t)$. Subtraction of the estimator (39) from the system (20) yields the following estimation error dynamics

$$\begin{aligned}\dot{\tilde{q}}(t) =& (\underline{\mu}D - L\tilde{H})\tilde{q}(t) + \mu_+ D\tilde{q}(t) + \tilde{\mu}Dq(t) \\ &+ [C\tilde{q}(t)]q(t) + [Cq(t)]\tilde{q}(t) - [C\tilde{q}(t)]\tilde{q}(t).\end{aligned} \tag{41}$$

where $\mu_+ := \mu - \underline{\mu} > 0$, and $\tilde{\mu} = \mu - \hat{\mu}$.

Our main result is presented in the following theorem.

*Theorem 2*

Consider the estimation error system (41). Let the observer gain $L$ be designed so that the matrix




DOI: 10.1002/acs

$\underline{\mu}D - L\tilde{H}$ is Hurwitz and satisfies the following property

$$\lambda_{\min}(Q) \geq 16 c_{\max} M \lambda_{\max}(P), \tag{42}$$

where $P = P^T > 0$ and $Q = Q^T > 0$ are the solutions of Lyapunov equation $P(\underline{\mu}D - L\tilde{H}) + (\underline{\mu}D - L\tilde{H})^T P^T = -Q$. Then, there exist positive constants $\rho_0 > 0$, $\rho_u > 0$, and a class $\mathcal{KL}$ function $\beta$ and a class $\mathcal{K}$ function $\gamma$ such that if $|\tilde{q}(0)| < \rho_0$ and $|\tilde{\mu}| < \rho_u$, then the following estimate of the norm holds :

$$||\tilde{q}(t)|| \leq \beta(||\tilde{q}(0)||, t) + \gamma\left(|\tilde{\mu}|\right), \tag{43}$$

which guarantees the local input-to-state stability (LISS) of the estimation error system with respect to the parameter uncertainty. Moreover, by defining $\bar{\sigma} = \frac{\lambda_{\min}(Q)}{4\sqrt{\lambda_{\min}(P)}\sqrt{\lambda_{\max}(P)}}$, $\bar{\delta} = c_{\max}\frac{\lambda_{\max}(P)}{\lambda_{\min}(P)^{3/2}}$, and $\bar{\alpha} = \frac{M\lambda_{\max}(P)}{\sqrt{\lambda_{\min}(P)}}\lambda_{\max}(-D)$ , the explicit formulation for the constant bound and functions are obtained by $\rho_u = \frac{\lambda_{\min}(Q)}{4\sqrt{\lambda_{\min}(P)}\sqrt{\lambda_{\max}(P)}}$, $\rho_0 = \frac{\bar{\sigma}}{4\bar{\delta}}$, and

$$\beta(||q_0||, t) = 4||q_0|| e^{-\frac{\bar{\sigma}}{2}t}, \tag{44}$$

$$\gamma(u) = 5\frac{\bar{\sigma} - \sqrt{\bar{\sigma}^2 - 4\sqrt{2}\bar{\delta}\bar{\alpha}u}}{2\bar{\delta}}, \tag{45}$$

which ensures the exponentially LISS.

*Proof*

We consider the candidate of LISS Lyapunov function $V$ defined by

$$\tilde{V} = \tilde{q}^T P \tilde{q} \tag{46}$$

Note $\lambda_{\min}(P)\tilde{q}^T\tilde{q} \leq \tilde{V} \leq \lambda_{\max}(P)\tilde{q}^T\tilde{q}$. Taking the time derivative of (46) along the solution of (41), we obtain

$$\begin{aligned}\dot{\tilde{V}} =& -\tilde{q}^T Q \tilde{q} + 2\tilde{\mu} q^T D^T P \tilde{q} - \tilde{\mu}\tilde{q}^T(DP + PD)\tilde{q} \\ &+ 2\mu_+ \tilde{q}^T DP\tilde{q} + 2\left([C\tilde{q}]q\right)^T P\tilde{q} + 2\left([Cq]\tilde{q}\right)^T P\tilde{q} \\ &- 2\left([C\tilde{q}]\tilde{q}\right)^T P\tilde{q}\end{aligned} \tag{47}$$

Owing to the negative definiteness of $D < 0$ and positivity of $\mu_+ > 0$, it holds $\mu_+\tilde{q}^T DP\tilde{q} < 0$. Furthermore, by Cauchy-Schwarz inequality,

$$\begin{aligned}\left([C\tilde{q}]q\right)^T P\tilde{q}, &\leq ||[C\tilde{q}]q|| \cdot ||P\tilde{q}|| \\ &\leq c_{\max}\lambda_{\max}(P) M ||\tilde{q}||^2,\end{aligned} \tag{48}$$




DOI: 10.1002/acs

where we used $||q|| \leq M$ given in Lemma 1. Using the same technique to all terms in the last line in (61), and defining $\bar{d} := \lambda_{\max}(-D) > 0$, the inequality (47) leads to

$$\begin{aligned}\dot{\tilde{V}} \leq & -\lambda_{\min}(Q)||\tilde{q}||^2 + 2M\bar{d}\lambda_{\max}(P)||\tilde{q}|||\tilde{\mu}| + 4c_{\max}\lambda_{\max}(P)M||\tilde{q}||^2 + 2c_{\max}\lambda_{\max}(P)||\tilde{q}||^3 \\ & + 2\lambda_{\min}(P)\bar{d}|\tilde{\mu}|||\tilde{q}||^2, \\ \leq & -\frac{\lambda_{\min}(Q)}{2}||\tilde{q}||^2 + 2c_{\max}\lambda_{\max}(P)||\tilde{q}||^3 + \left(2M\bar{d}\lambda_{\max}(P)|\tilde{\mu}| - \frac{\lambda_{\min}(Q)}{4}||\tilde{q}||\right)||\tilde{q}|| \\ & + \left(4c_{\max}\lambda_{\max}(P)M - \frac{\lambda_{\min}(Q)}{4}\right)||\tilde{q}||^2 + 2\lambda_{\min}(P)\bar{d}|\tilde{\mu}|||\tilde{q}||^2. \end{aligned} \tag{49}$$

Therefore, by designing the observer gain $L$ such that the condition (42) holds, we can state that if

$$|\tilde{\mu}| \leq p||\tilde{q}||, \tag{50}$$

where $p := \frac{\lambda_{\min}(Q)}{16M\bar{d}\lambda_{\max}(P)}$, then (49) leads to

$$\dot{\tilde{V}} \leq -\sigma||\tilde{q}||^2 + \delta||\tilde{q}||^3, \tag{51}$$

where $\sigma = \frac{\lambda_{\min}(Q)}{2}$, $\delta = 2\lambda_{\max}(P)\left(c_{\max} + \bar{d}p\right)$. Applying Theorem 1 in [9], we can conclude the local ISS w.r.t. the parameter uncertainty $\mu$. Applying the similar technique in proof of Lemma 1 to (49), we can further obtain the explicit bound by the solution of Riccati differential equation, which derive the explicit formulation of the functions $\beta$ and $\gamma$ in LISS. □

### *4.2. Observer based on the ROM-CL model*

Similarly to (39), the Luenberger-like observer in this case is written as

$$\dot{\hat{q}}(t) = \hat{\mu}_{\rm cl}D\hat{q}(t) + [C\hat{q}(t)]\hat{q}(t) + b + \hat{\mu}_{\rm nl}(c_{\max}||\hat{q}||^2 + b_{\max})D^*\hat{q} + L(y(t) - \tilde{H}\hat{q}(t)), \tag{52}$$

where $\hat{\mu}_{\rm nl}$ is the estimated value of $\mu_{\rm nl}$. Subtraction of the estimator (52) from ROM-CL system (37) yields the following system for the estimation error state $\tilde{q}(t) := q(t) - \hat{q}(t)$ :

$$\begin{aligned}\dot{\tilde{q}}(t) = & A\tilde{q}(t) + (\mu_{+,\rm cl}D + \mu_{+,\rm nl}D^*)\tilde{q}(t) + \tilde{\mu}_{\rm cl}Dq(t) + [Cq(t)]q(t) - [C\hat{q}(t)]\hat{q}(t) \\ & + \hat{\mu}_{\rm nl}c_{\max}(||q||^2D^*q(t) - ||\hat{q}||^2D^*\hat{q}(t)) + \tilde{\mu}_{\rm nl}(c_{\max}||q||^2 + b_{\max})D^*q(t). \end{aligned} \tag{53}$$

where $A := \underline{\mu}_{\rm cl}D + \underline{\mu}_{\rm nl}b_{\max}D^* - LH$. The last two terms in (53) are calculated as

$$\begin{aligned}[Cq(t)]q(t) - [C\hat{q}(t)]\hat{q}(t) = & [Cq(t)]q(t) - [C(q(t) - \tilde{q}(t))](q(t) - \tilde{q}(t)), \\ = & [C\tilde{q}(t)]q(t) + [Cq(t)]\tilde{q}(t) - [C\tilde{q}(t)]\tilde{q}(t). \end{aligned} \tag{54}$$

$$\begin{aligned}||q||^2D^*q - ||\hat{q}||^2D^*\hat{q} = & ||q||^2D^*q - (q - ||q||\tilde{q})^T(q - \tilde{q})D^*(q - \tilde{q}), \\ = & ||q||^2D^*q - (||q||^2 - 2\tilde{q}^Tq + ||\tilde{q}||^2)D^*(q - \tilde{q}), \\ = & (2\tilde{q}^Tq - ||\tilde{q}||^2)D^*q + ||\hat{q}||^2D^*\tilde{q}. \end{aligned} \tag{55}$$




DOI: 10.1002/acs

Substituting (54) into (53), the estimation error dynamics is written as

$$\begin{aligned}\dot{\tilde{q}}(t) =& A\tilde{q}(t) + (\mu_{+,\mathrm{cl}}D + \mu_{+,\mathrm{nl}}D^*)\tilde{q}(t) + \tilde{\mu}_{\mathrm{cl}}Dq(t) + [C\tilde{q}(t)]q(t) + [Cq(t)]\tilde{q}(t) - [C\tilde{q}(t)]\tilde{q}(t) \\ &+ \hat{\mu}_{\mathrm{nl}}c_{\max}((2\tilde{q}^Tq - ||\tilde{q}||^2)D^*q + ||\hat{q}||^2D^*\tilde{q}) + \tilde{\mu}_{\mathrm{nl}}(c_{\max}||q||^2 + b_{\max})D^*q(t). \end{aligned} \tag{56}$$

To validate the performance of the designed estimator, we aim to prove the stability of the estimation error state $\tilde{q}$ governed by the differential equation in (56). Analogously to Theorem 2, a theoretical result for ROM-CL is presented in the following theorem.

*Theorem 3*

Consider the estimation error system (56) and let $\tilde{\mu} \in \mathbb{R}^2$ be a vector of parameters' error defined by $\tilde{\mu} = (\tilde{\mu}_{\mathrm{cl}}, \tilde{\mu}_{\mathrm{nl}})^T$. Let design the observer gain $L$ such that the system matrix $A := \underline{\mu}_{\mathrm{cl}}D + \underline{\mu}_{\mathrm{nl}}b_{\max}D^* - LH$ is Hurwitz matrix and having the property

$$\lambda_{\min}(Q) \geq 16c_{\max}\lambda_{\max}(P)M(1 + M\bar{d}\hat{\mu}_{\mathrm{nl}}), \tag{57}$$

where $P = P^T > 0$ and $Q = Q^T > 0$ are the solutions of Lyapunov equation $PA + A^TP^T = -Q$. There exists positive constants $\rho_0 > 0$, $\rho_u > 0$, and a class $\mathcal{KL}$ function $\beta$ and a class $\mathcal{K}$ function $\gamma$ such that if $||\tilde{q}(0)|| < \rho_0$ and $||\tilde{\mu}|| < \rho_u$, then the following estimate of the norm holds :

$$||\tilde{q}(t)|| \leq \beta(||\tilde{q}(0)||, t) + \gamma\left(||\tilde{\mu}||\right), \tag{58}$$

which guarantees the local input-to-state stability (LISS) of the estimation error system with respect to the multi parametric uncertainties.

*Proof*

The proof of Theorem 3 is analogous to the proof of Theorem 2. Namely, we consider the candidate of LISS Lyapunov function $V$ defined by

$$V = \tilde{q}^TP\tilde{q}. \tag{59}$$

Let $f_1(\tilde{q}, \tilde{\mu}_{\mathrm{cl}})$ be defined by the first line of RHS in (56), and $f_2(\tilde{q}, \hat{\mu}_{\mathrm{nl}}, \tilde{\mu}_{\mathrm{nl}})$ be defined by the second line of RHS. Taking the time derivative of (59), we obtain

$$\dot{V} = f_1(\tilde{q}, \tilde{\mu}_{\mathrm{cl}})^TP\tilde{q} + \tilde{q}^TPf_1(\tilde{q}, \tilde{\mu}_{\mathrm{cl}}) + f_2(\tilde{q}, \hat{\mu}_{\mathrm{nl}}, \tilde{\mu}_{\mathrm{nl}})^TP\tilde{q} + \tilde{q}^TPf_2(\tilde{q}, \hat{\mu}_{\mathrm{nl}}, \tilde{\mu}_{\mathrm{nl}}) \tag{60}$$

Then, we have

$$\begin{aligned}& f_1(\tilde{q}, \tilde{\mu}_{\mathrm{cl}})^TP\tilde{q} + \tilde{q}^TPf_1(\tilde{q}, \tilde{\mu}_{\mathrm{cl}}) \\ =& \{A\tilde{q}(t) + (\mu_{+,\mathrm{cl}}D + \mu_{+,\mathrm{nl}}D^*)\tilde{q}(t) + \tilde{\mu}_{\mathrm{cl}}Dq(t) + [C\tilde{q}(t)]q(t) + [Cq(t)]\tilde{q}(t) - [C\tilde{q}(t)]\tilde{q}(t)\}^TP\tilde{q} \\ &+ \tilde{q}^TP\{A\tilde{q}(t) + (\mu_{+,\mathrm{cl}}D + \mu_{+,\mathrm{nl}}D^*)\tilde{q}(t) + \tilde{\mu}_{\mathrm{cl}}Dq(t) + [C\tilde{q}(t)]q(t) + [Cq(t)]\tilde{q}(t) - [C\tilde{q}(t)]\tilde{q}(t)\}, \\ =& -\tilde{q}^TQ\tilde{q} + \tilde{q}^T\bar{D}\tilde{q} + 2\tilde{\mu}_{\mathrm{cl}}q^TD^TP\tilde{q} + \left([C\tilde{q}]q\right)^TP\tilde{q} + \left([Cq]\tilde{q}\right)^TP\tilde{q} - \left([C\tilde{q}]\tilde{q}\right)^TP\tilde{q} \\ &+ \tilde{q}^TP([C\tilde{q}]q) + \tilde{q}^TP([Cq]\tilde{q}) - \tilde{q}^TP([C\tilde{q}]\tilde{q}), \end{aligned} \tag{61}$$



*Prepared using* acsauth.cls
DOI: 10.1002/acs

where

$$\bar{D} = (\mu_{+,\mathrm{cl}} D + \mu_{+,\mathrm{nl}} D^*)^T P + P(\mu_{+,\mathrm{cl}} D + \mu_{+,\mathrm{nl}} D^*) < 0, \tag{62}$$

and hence $\tilde{q}^T \bar{D} \tilde{q} < 0$. By Cauchy-Schwarz inequality,

$$([C\tilde{q}]q)^T P\tilde{q} \leq |[C\tilde{q}]q|| \cdot ||P\tilde{q}|| \leq |[C\tilde{q}]q||\lambda_{\max}(P)||\tilde{q}||. \tag{63}$$

For all $a \in \mathbb{R}^n$ and $b \in \mathbb{R}^n$, it holds that

$$|[Ca]b|| \leq c_{\max}||a|| \cdot ||b||. \tag{64}$$

Applying (64) to (63) with the help of $||q|| < M$, we obtain

$$([C\tilde{q}]q)^T P\tilde{q} \leq c_{\max}\lambda_{\max}(P)M||\tilde{q}||^2. \tag{65}$$

Using the same technique to all terms in the last two lines in (61) yields

$$\begin{aligned}
&f_1(\tilde{q}, \tilde{\mu}_{\mathrm{cl}})^T P\tilde{q} + \tilde{q}^T P f_1(\tilde{q}, \tilde{\mu}_{\mathrm{cl}}) \\
\leq& -\lambda_{\min}(Q)||\tilde{q}||^2 + 2M\lambda_{\max}(-D)\lambda_{\max}(P)||\tilde{q}|||\tilde{\mu}_{\mathrm{cl}}| \\
&+ 4c_{\max}\lambda_{\max}(P)M||\tilde{q}||^2 + 2c_{\max}\lambda_{\max}(P)||\tilde{q}||^3, \\
\leq& -\frac{\lambda_{\min}(Q)}{2}||\tilde{q}||^2 + \left(2M\lambda_{\max}(-D)\lambda_{\max}(P)|\tilde{\mu}_{\mathrm{cl}}| - \frac{\lambda_{\min}(Q)}{4}||\tilde{q}||\right)||\tilde{q}|| \\
&+ \left(4c_{\max}\lambda_{\max}(P)M - \frac{\lambda_{\min}(Q)}{4}\right)||\tilde{q}||^2 + 2c_{\max}\lambda_{\max}(P)||\tilde{q}||^3.
\end{aligned} \tag{66}$$

Next, we consider

$$\begin{aligned}
&f_2(\tilde{q}, \hat{\mu}_{\mathrm{nl}}, \tilde{\mu}_{\mathrm{nl}})^T P\tilde{q} + \tilde{q}^T P f_2(\tilde{q}, \hat{\mu}_{\mathrm{nl}}, \tilde{\mu}_{\mathrm{nl}}) \\
=&\hat{\mu}_{\mathrm{nl}}c_{\max}\left\{||\hat{q}||^2\tilde{q}^T\bar{D}\tilde{q} + (2\tilde{q}^T q - ||\tilde{q}||^2)(q^T D^{*T} P\tilde{q} + \tilde{q}^T P D^* q)\right\} \\
&+ \tilde{\mu}_{\mathrm{nl}}(c_{\max}||q||^2 + b_{\max})(\tilde{q}^T P D^* q + q^T D^{*T} P\tilde{q}),
\end{aligned} \tag{67}$$

where

$$\bar{\bar{D}} = D^{*T} P + P D^* < 0, \tag{68}$$

and therefore $||\hat{q}||^2\tilde{q}^T\bar{\bar{D}}\tilde{q} < 0$. Also, using $||q|| < M$, we have

$$q^T D^{*T} P\tilde{q} + \tilde{q}^T P D^* q \leq 2M\lambda_{\max}(P)\bar{d}||\tilde{q}||, \tag{69}$$

where $\bar{d} = \max_i\{-d_{ii}\} > 0$. Applying the same technique to all terms in (67), we get

$$\begin{aligned}
&f_2(\tilde{q}, \hat{\mu}_{\mathrm{nl}}, \tilde{\mu}_{\mathrm{nl}})^T P\tilde{q} + \tilde{q}^T P f_2(\tilde{q}, \hat{\mu}_{\mathrm{nl}}, \tilde{\mu}_{\mathrm{nl}}) \\
\leq& 2M\lambda_{\max}(P)\bar{d}\hat{\mu}_{\mathrm{nl}}c_{\max}(2M||\tilde{q}||^2 + ||\tilde{q}||^3) \\
&+ 2M\lambda_{\max}(P)\bar{d}(c_{\max}M^2 + b_{\max})|\tilde{\mu}_{\mathrm{nl}}| \cdot ||\tilde{q}||.
\end{aligned} \tag{70}$$




DOI: 10.1002/acs

Finally, applying (66) and (70) to (60) leads to

$$\begin{aligned}\dot{V} \leq & -\frac{\lambda_{\min}(Q)}{2}||\tilde{q}||^2 \\ & + \left(2M\lambda_{\max}(-D)\lambda_{\max}(P)|\tilde{\mu}_{\rm cl}| - \frac{\lambda_{\min}(Q)}{8}||\tilde{q}||\right)||\tilde{q}|| \\ & + \left(2M\lambda_{\max}(P)\bar{d}(c_{\max}M^2 + b_{\max})|\tilde{\mu}_{\rm nl}| - \frac{\lambda_{\min}(Q)}{8}||\tilde{q}||\right)||\tilde{q}|| \\ & + \left(4c_{\max}\lambda_{\max}(P)M(1 + M\bar{d}\hat{\mu}_{\rm nl}) - \frac{\lambda_{\min}(Q)}{4}\right)||\tilde{q}||^2 \\ & + 2c_{\max}\lambda_{\max}(P)(1 + M\bar{d}\hat{\mu}_{\rm nl})||\tilde{q}||^3. \end{aligned} \tag{71}$$

Therefore, by designing the observer gain $L$ such that the condition (57) holds, we can state that if

$$||\tilde{q}|| \geq p||\tilde{\mu}||, \tag{72}$$

where $p := \frac{16M\lambda_{\max}(P)}{\lambda_{\min}(Q)} \max\{\lambda_{\max}(-D), \bar{d}(c_{\max}M^2 + b_{\max})\}$, then (71) leads to

$$\dot{V} \leq -\sigma||\tilde{q}||^2 + \delta||\tilde{q}||^3, \tag{73}$$

where

$$\sigma = \frac{\lambda_{\min}(Q)}{2}, \quad \delta = 2c_{\max}\lambda_{\max}(P)(1 + M\bar{d}\hat{\mu}_{\rm nl}). \tag{74}$$

Hence, similarly to the end of proof of Theorem 2, we can conclude the local ISS w.r.t. the multi parametric uncertainties. □

*Remark 3*

Our present work develops a state observer for ROM of the original PDE and analyzes the stability of only the ROM-based observer dynamics, which does not guarantee a rigorous analysis with respect to the original PDE model. Indeed, [24] analyzes the norm of the state observer with respect to the full space of the original PDE model, while the design procedure is distinct from our present work, we will consider such a norm analysis for our observer design in our future work.

## 5. PARAMETRIC UNCERTAINTY ESTIMATION BY AN EXTREMUM SEEKING ALGORITHM

To enhance the performance of the state observer (39) or (52), based on the measured value, the uncertain parameters estimate $\hat{\mu} = (\hat{\mu}_{\rm cl},\ \hat{\mu}_{\rm nl})^T \in \mathbb{R}^2$ in (52) for ROM-CL, or simply $\hat{\mu} \in \mathbb{R}$ in (39) for ROM-G, used in the observer should be corrected through learning iterations. The learning cost function to minimize at every iteration is an error between the measured value and its estimate, which is formulated as

$$Q(\hat{\mu}) = \int_0^{t_f} (y(t) - \tilde{H}\hat{q}(t))^T R(y(t) - \tilde{H}\hat{q}(t))dt,\ R > 0. \tag{75}$$




DOI: 10.1002/acs

Since the estimate of the parameter $\hat{\mu}$ affects the observer state $\hat{q}$, the cost function $Q$ is an implicit function of $\hat{\mu}$. Following [5], we impose the following assumptions on the cost function.

*Assumption 3*

The cost function $Q(\cdot)$ in (75) has a local minimum at $\hat{\mu} = \mu$.

*Assumption 4*

The cost function in (75) is analytic and its variation with respect to $\hat{\mu}$ is bounded in the neighborhood of $\mu$, i.e., $||\nabla_{\hat{\mu}} Q(\delta\mu)|| \leq \xi_2,\ \xi_2 > 0$, for all $\delta\mu \in \mathcal{N}(\mu)$, where $\mathcal{N}(\mu)$ denotes a compact neighborhood of $\mu$.

We apply an extremum seeking algorithm as a learning method for parameter identification. Let $\hat{\mu}^{(i)}$ be the estimate of the parameter $\mu$ at $i$-th iteration, and we introduce an internal variable $z^{(i)}$ with initial value $z^{(1)} = \hat{\mu}^{(1)}$. The parameters update through ES algorithm is given by

$$z_1^{(i+1)} = z_1^{(i)} + a_1 \delta \sin\left(\omega_1 i\delta + \frac{\pi}{2}\right) Q(\hat{\mu}^{(i)}) \tag{76}$$

$$\hat{\mu}_{\mathrm{cl}}^{(i+1)} = z_1^{(i+1)} + a_1 \sin\left(\omega_1 i\delta - \frac{\pi}{2}\right) \tag{77}$$

$$z_2^{(i+1)} = z_2^{(i)} + a_2 \delta \sin\left(\omega_2 i\delta + \frac{\pi}{2}\right) Q(\hat{\mu}^{(i)}) \tag{78}$$

$$\hat{\mu}_{\mathrm{nl}}^{(i+1)} = z_2^{(i+1)} + a_2 \sin\left(\omega_2 i\delta - \frac{\pi}{2}\right), \tag{79}$$

where the tuning parameters are $(a_1, \omega_1, a_2, \omega_2, \delta)$ which are the amplitude, the frequency, and the iteration increment $\delta > 0$, respectively. Owing to the convergence analysis of the extremum seeking algorithm as presented for example in [14, 5], the performance of the learning-based observer is addressed in the following lemma.

*Lemma 3*

Let Assumptions 2–4 hold. Consider the ROM-CL (37) and the designed observer (52) satisfying (57). Furthermore, where the viscosity estimate $\hat{\mu}$ is tuned by the ES algorithm (76)-(79) associated with the cost function (75) at the iteration step $i \in \mathbb{N}$. Then, there exists $\xi_1 > 0$ such that the norm of the parameter estimation error and the learning cost function admit the following bounds

$$\limsup_{i\to\infty} ||\hat{\mu}^{(i)} - \mu|| \leq \frac{\xi_1}{\omega} + ||a||, \tag{80}$$

$$\limsup_{i\to\infty} |Q(\hat{\mu}^{(i)}) - Q(\mu)| \leq \xi_2 \left(\frac{\xi_1}{\omega} + ||a||\right), \tag{81}$$

where $a = (a_1,\ a_2)^T$, and $\omega = \max\{\omega_1,\ \omega_2\}$. Moreover, if $||\tilde{q}(0)|| < \rho_0$ and $||\tilde{\mu}|| < \rho_u$ then the norm of the state estimation error admits the following bound

$$\limsup_{i\to\infty} ||\tilde{q}^{(i)}(t)|| \leq \beta(||\tilde{q}_0||, t) + \gamma\left(\frac{\xi_1}{\omega} + ||a||\right) \tag{82}$$

where $\tilde{q}^{(i)}(t) = q(t) - \hat{q}^{(i)}(t)$ with the observer state $\hat{q}^{(i)}(t)$ in $i$-th iteration, $\rho_0$, $\rho_u$, $\beta$, and $\gamma$ are defined in both Theorems 2 and 3.




DOI: 10.1002/acs

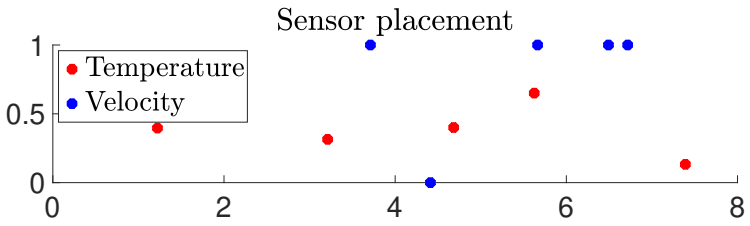


Figure 1: Sensor placement for both temperature (red) and velocity (blue).

*Proof*

The proof of (80) and (81) is the same derivation as in [4], and hence is omitted here. Finally, taking the supremum limit in the norm bound (58) in Theorem 3, we obtain

$$\limsup_{i\to\infty} ||\tilde{q}^{(i)}(t)|| \leq \beta(||\tilde{q}_0||, t) + \limsup_{i\to\infty} \gamma\left(||\mu - \hat{\mu}^{(i)}||\right) \tag{83}$$

from which the norm estimate (82) is derived with the help of (80). □

*Remark 4*

The result of Lemma 3 are obviously valid for the case of a scalar parameter $\hat{\mu}$ in the case of the ROM-G (20), and its ROM-G observer (52), under condition (42).

*Remark 5*

Note that, due to the LISS results, the proposed method is modular, in the sense that one could use other learning algorithms to estimate the viscosity parameter. For instance, we can readily use other ES algorithms, with no residual oscillations, e.g., [26], or with vanishing perturbations, e.g., [17]. One could also use Bayesian optimization methods, e.g., GP-UCB [27].

## 6. NUMERICAL SIMULATION

### *6.1. Numerical solvers for the 2D Boussinesq equations*

The numerical solution for the 2D Rayleigh-Benard convection problem follows the scheme outlined in [19]. Compact fourth-order Padé finite difference schemes are used for the spatial derivatives as in [20]. The first derivative is approximated using the stencil

$$\alpha f'_{i-1} + f'_i + \alpha f'_{i+1} = \frac{a}{2h}\left(f_{i+1} - f_{i-1}\right)$$

with $\alpha = 1/4$ and $a = \frac{2}{3}(\alpha + 2)$. The second derivative is approximated using the stencil

$$\alpha f''_{i-1} + f''_i + \alpha f''_{i+1} = \frac{a}{h^2}\left(f_{i+1} - 2f_i + f_{i-1}\right)$$

with $\alpha = 1/10$ and $a = \frac{4}{3}(1 - \alpha)$. Time integration is performed using the optimal third-order total variation diminishing Runge-Kutta (TVDRK3) scheme given in [21]. The stream function $\psi$ can be



*Prepared using* acsauth.cls
DOI: 10.1002/acs

obtained from the vorticity using the Poisson equation

$$\frac{\partial^2 \psi}{\partial x^2} + \frac{\partial^2 \psi}{\partial y^2} = -\omega.$$

This is solved using the Mehrstellen scheme [22].

### *6.2. Input parameters*

We implement the numerical simulation by setting the spatial domain as a 2-D rectangular shape, namely, $\Omega = (0, 8) \times (0, 1)$. The non-dimensional parameters are chosen as Re $= 10^4$, Pr $= 1$, and Gr $= 4 \times 10^8$. The setup of this experiment, e.g., [4] , is as follows: Two fluids of different temperatures are separated by a vertical barrier at $x = 4$. On the right side of the barrier we have low temperature set to $1$, whereas, on the left side of the barrier we have high temperature, set to $1.5$. When we remove the barrier between the two fluids, we expect the low density, warmer fluid to rise, while the high density, cooler fluid sinks. The flow is at rest initially (i.e., the vorticity and stream functions are set to zero at $t = 0$) with constant temperature values for the left and right fluids. The 2-D equations were simulated using a vorticity-stream function formulation with no-slip boundary conditions for vorticity and adiabatic boundary conditions for temperature. We use 10 POD basis functions for the vorticity and 10 POD basis functions for the temperature variables computed from snapshots taken every $2 \times 10^{-2}$[s]. The simulation time is set as $t_f$ =10 [s]. In Figures 2, and 3, we present the direct numerical simulation (DNS) of (8)-(10). We show two snapshots, one close to the initial simulation time, and one close to the final simulation time. The first snapshot, shown in Figure 2, is taken at the initial instant $t = 2 \times 10^{-2}$ $[sec]$ (to avoid the trivial snapshot corresponding to $t = 0$ $sec$ showing the static boundary conditions), the second snapshot, shown in Figure 3, corresponds to $t = 8[sec]$. One case see the mixing happening after the removal of the barrier between the two fluids, which makes this case a challenging fluid dynamics example.

The observer gain is obtained using an LMI solver in MATLAB to ensure the existence of a positive solution to the Lyapunov equation stated in Theorem 2. For measurements, we consider 5 sensors for temperature and 5 sensors for velocity, and they are placed, using Q-DEIM method, e.g., [7], at the locations which are depicted in Fig. 1. Then, the measurement matrix $\tilde{H}$ in (38) is obtained through the POD basis functions.

### *6.3. Algorithm for ES-based observer*

After time discretization, the dynamics of the ROM-G (20) and the designed observer (39) (or the ROM-CL (37), and its observer (52)) are described by the difference equation in the form of $\hat{q}_{k+1} = f(\hat{q}_k, y_k, \hat{\mu})$, for $k = 0, 1, \cdots, T_f$, with $\hat{q}_k = \hat{q}(k\Delta t)$ and $T_f = t_f/\Delta t$. In numerical experiment, the measured values $\{y_k\}_{k=0}^{T_f}$ are obtained through forward simulation of the model. Using the collected measured data as inputs, we calculate the observer state $\{\hat{q}_k\}_{k=0}^{T_f}$ with an initial




DOI: 10.1002/acs

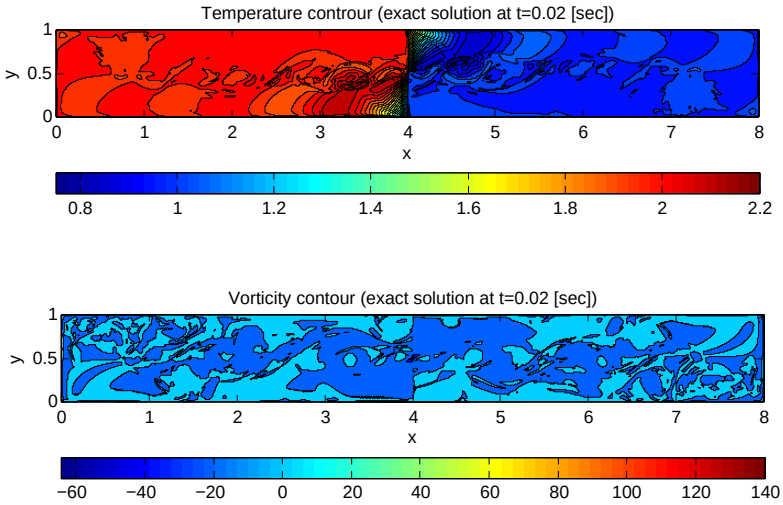


Figure 2: True solution profile snapshot at $0.02[sec]$ (top: temperature, bottom: vorticity)

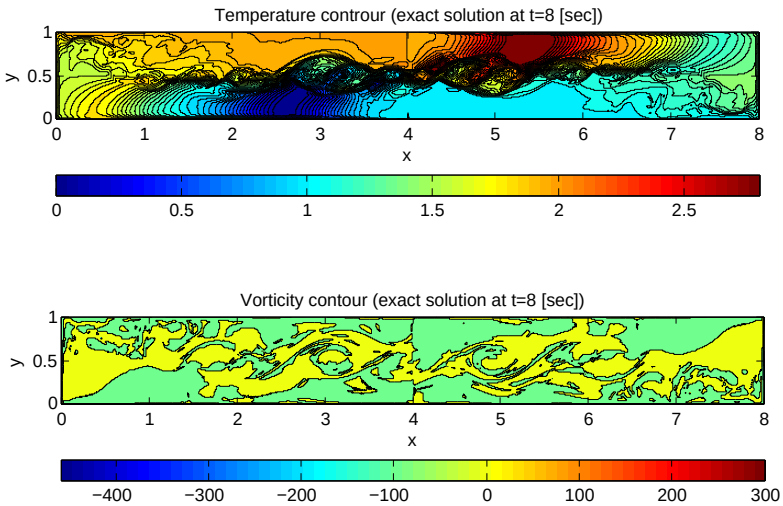


Figure 3: True solution profile snapshot at $8[sec]$ (top: temperature, bottom: vorticity)

guess of $\hat{\mu}$. Once $\{\hat{q}_k\}_{t=0}^{T_f}$ has been obtained, the ES algorithm is implemented to update the learned parameter. We repeat this process ("run observer" $\leftrightarrow$ "parameter update") up to $I$-th iterations, where $I$ is a chosen iteration number. After that, the averaged value of the learned parameter over the last 10 % steps is calculated, which serves as the value for the uncertain parameter estimate. Finally, we run the observer dynamics again, using the learned parameter. This procedure is stated in Algorithm 1.



*Prepared using* acsauth.cls
DOI: 10.1002/acs

**Algorithm 1:** Iterative learning for online parameter estimation in state observer

**Input :** $\{y_k\}_{k=0}^{T_f}$ , $\hat{\mu}^{(1)}$ , $\hat{q}_0$;

$z \leftarrow \hat{\mu}^{(1)}$;

**for** $i = 1, 2, \cdots, I$, **do**

  **for** $k = 0, \cdots, t_f - 1$, **do**

    $\hat{q}_{k+1} \leftarrow f(\hat{q}_k, y_k, \hat{\mu}^{(i)})$;

    $\tilde{y}_k \leftarrow y_k - H\hat{q}_k$;

  **end for**

  $Q \leftarrow \text{Trapz}\{\tilde{y}_k^T \tilde{y}_t\}_{k=0}^{T_f}$ ;

  $z \leftarrow z + a\delta \sin\left(\omega i\delta + \frac{\pi}{2}\right) Q$;

  $\hat{\mu}^{(i+1)} \leftarrow z + a \sin\left(\omega i\delta - \frac{\pi}{2}\right)$ ;

**end for**

$\hat{\mu}^{\text{ave}} \leftarrow \text{Mean}\left(\{\hat{\mu}^{(i)}\}_{i=0.9\cdot I}^{I}\right)$;

**for** $k = 0, \cdots, T_f - 1$, **do**

  $\hat{q}_{k+1} \leftarrow f(\hat{q}_k, y_k, \hat{\mu}^{\text{ave}})$;

**end for**

**Output :** $\hat{\mu}^{\text{ave}}$, $\{\hat{q}_k\}_{k=0}^{T_f}$

### *6.4. Simulation result*

*6.4.1. Case of the observer based on ROM-G:* In these tests, the initial observer state is set as $\hat{q}(0) = (1 + \varepsilon)q(0)$, with setting $\varepsilon = 0.1$, which implies that the observer state has 10 % error on the initial conditions. The true viscosity is normalized as $\mu = 1.0$, while the initial guess of the estimated viscosity is set as $\hat{\mu}^{(1)} = 0.85$, which has 15% error. The parameters of dither signals are set as $a_1 = 0.02$, $\omega_1 = 1000$, and $\delta = 0.001$, respectively. The learned parameter is updated through 1000 iterations.

The simulation of the learning-based observer is implemented. Fig. 4 depicts the time evolution of the first two modes in both velocity and temperature for the: true value (red), estimate before learning (green), and the estimate after learning (blue), respectively. For all of these four states, we can observe that the estimated value becomes much closer to the true value after ES-based learning of the uncertain parameter. As depicted in Fig. 5, the norm of the estimation error is converging to zero after learning (blue), while the estimation error norm before learning shows a diverging behavior.

The update of the learned parameter $\hat{\mu}^{(i)}$ over the learning iterations is depicted in Fig. 6 (left). While the initial guess of the parameter has 15% error, by employing ES we can observe that after 200 steps the learned parameter $\hat{\mu}^{(i)}$ converges to the neighborhood of the true value $\hat{\mu}$. The




DOI: 10.1002/acs

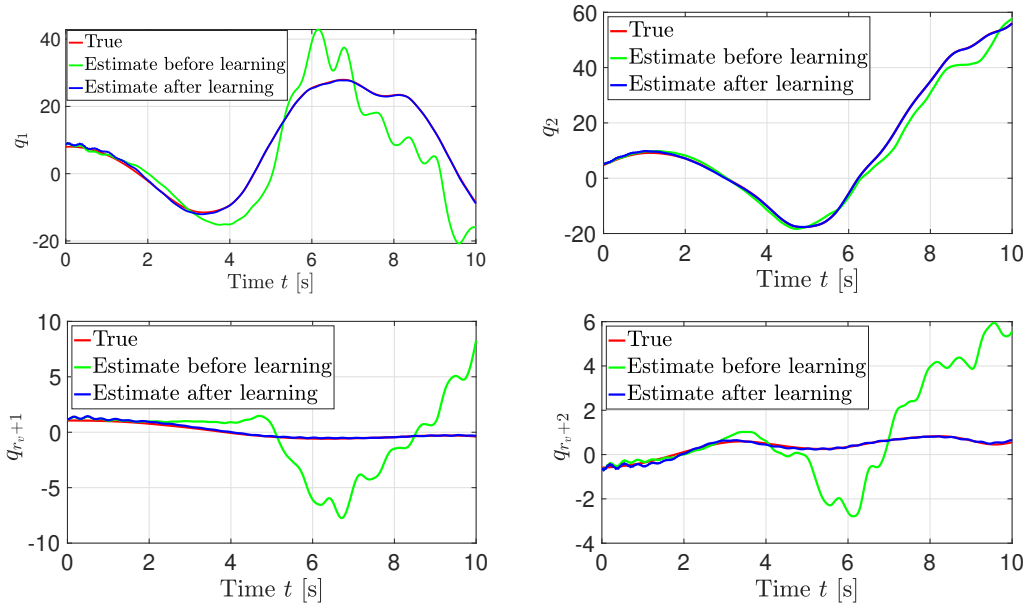


Figure 4: Evolution of first and second modes in both velocity and temperature states of ROM-G: True value (red), estimate before learning (green), and estimate after learning (blue). For all of the modes given here, we can observe that the estimate value is highly improved after learning the uncertain parameter.

amplitude of the learned parameter around the averaged value directly depends on the amplitude $a$ of the dither signal for ES, which can be tuned by the user. Smaller choice of $a$ decreases the amplitude of the learned parameter, however, the convergence speed becomes slower in general. Such a tradeoff can be dealt by performance improvement of the ES algorithm proposed in [17], which provides convergence to global optima in the presence of local extrema. Finally, the iterative update of the cost function is shown in Fig. 6 (right), from which we observe the convergence to the minimum value of $Q$ after 100 steps. Overall, the proposed method for a learning-based state estimation shows a good performance in this numerical study of the challenging 2-D Boussinesq equations.

However, for this challenging, near turbulent case, the states' norm of reduced order model ROM-G is diverging, for large time intervals, as depicted in Fig. 7, which violates the boundedness of the solution given in Lemma 1. This observation leads us to further study the performance of ROM-CL and its observer for the large time intervals.

*6.4.2. Case of the observer based on ROM-CL:* Next, we have studied the performance of the observer based on ROM-CL (52). Following the results in [4], the true (normalized) parameters are chosen as $\mu_{\mathrm{cl}} = 1.0$ and $\mu_{\mathrm{nl}} = 1.25 \cdot 10^{-3}$. The initial value of the learning parameters are



*Prepared using* acsauth.cls
DOI: 10.1002/acs

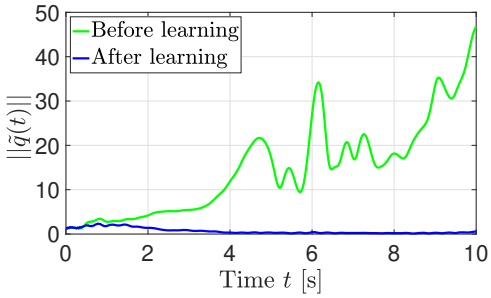


Figure 5: Comparison of the estimation error's norm before learning (green) and after learning (blue), which illustrates high improvement of the estimater performance through ES-based auto-tuning of parameter.

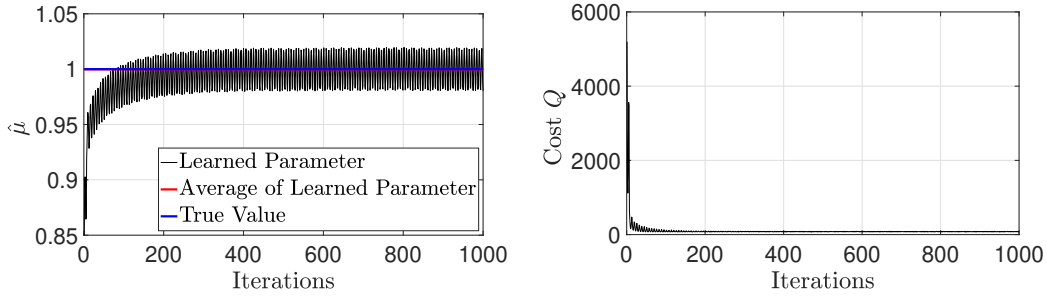


Figure 6: Updates of the learned parameter (left) and the cost value $Q$ (right) by ES through 1000 iterations. After 200 steps, the learned parameter $\hat{\mu}^{(i)}$ stays on neighborhood of the true value $\mu = 1.0$. The averaged value of the learned parameter over the last 100 steps becomes $\hat{\mu}^{\text{ave}} = 1.0$, same value as the true value. The value of the cost is largely decreased during the first 100 steps, and after that it maintains small oscillations around the minimum.

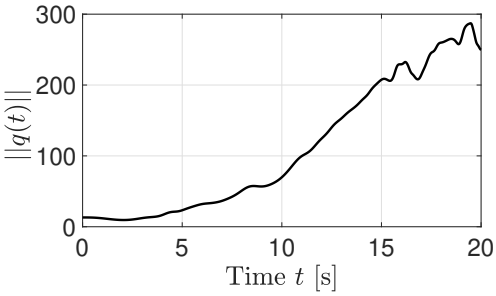


Figure 7: Divergence of ROM-G states' norm for large time interval is observed, which leads us to propose ROM-CL model and its observer.

$\hat{\mu}_{\text{cl}}^{(1)} = 0.8$ (20% error) and $\hat{\mu}_{\text{nl}}^{(1)} = 10^{-3}$ (20% error). The amplitudes and the frequencies of the dither signals in ES algorithm are set as $a_1 = 0.01$, $a_2 = 1.0 \cdot 10^{-4}$, $\omega_1 = 1000$, $\omega_2 = 1500$, with the



*Prepared using* acsauth.cls
DOI: 10.1002/acs

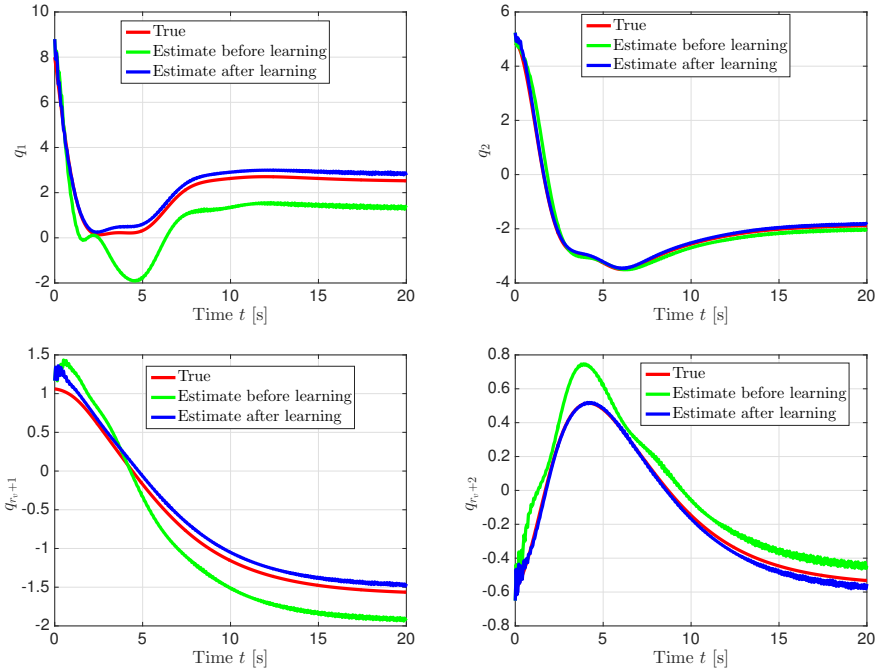


Figure 8: Evolution of first and second modes in both velocity and temperature states of ROM-CL: True value (red), estimate before learning (green), and estimate after learning (blue). We observe that the estimate value is highly improved after learning two parameters.

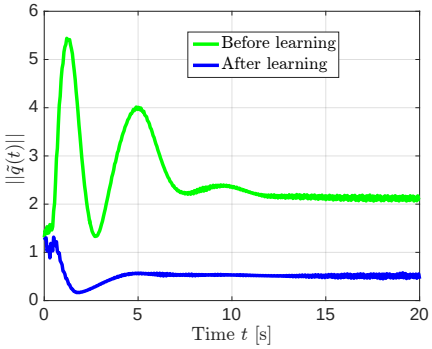


Figure 9: Comparison of the estimation error's norm before learning (green) and after learning (blue), which illustrates high improvement of the estimator's performance through multi-parametric ES-based learning.

iteration increment $\delta = 0.001$. We implemented the proposed learning-based estimation for ROM-CL with $5000$ iterations.

Fig. 8 depicts the time evolution of the first two modes in both velocity and temperature states of ROM-CL: true value (red), estimate before learning (green), and estimate after learning (blue). First, the boundedness of the true states is observed, which shows the expected effect of the closure




DOI: 10.1002/acs

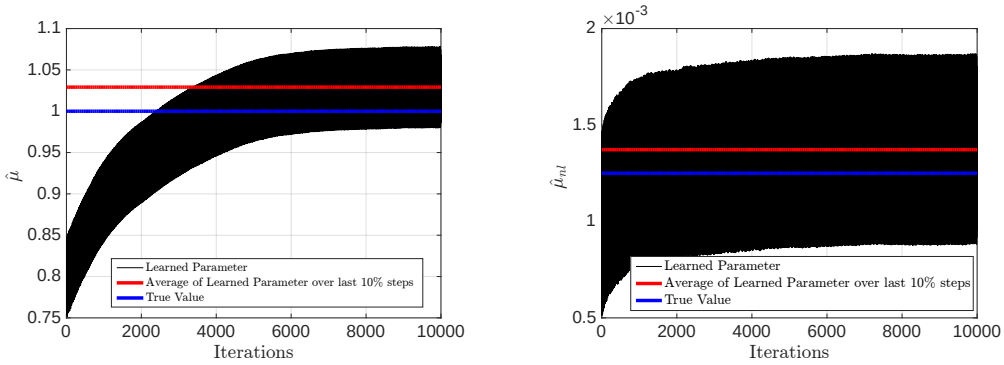


Figure 10: Updates of the learned parameters through multi-parametric ES: viscosity coefficient $\hat{\mu}_{\mathrm{cl}}$ (left) and ROM-CL's damping parameter $\hat{\mu}_{\mathrm{nl}}$ (right).

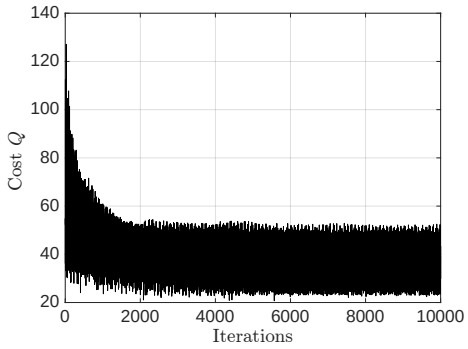


Figure 11: Decrease of the cost value through the parameters' learning.

model. Second, the estimated states becomes much closer to the true states after the multi-parametric ES-based learning of the uncertain parameters. The norm of the estimation error is depicted in Fig. 9 before learning (green) and after learning (blue), which illustrates the high improvement of the estimation through multi-parametric learning of uncertain parameters by ES.

Fig. 10 shows the updates of the learned parameters through the iterations: the viscosity coefficient $\hat{\mu}_{\mathrm{cl}}$ (left) and ROM-CL's damping parameter $\hat{\mu}_{\mathrm{nl}}$ (right). As observed from Fig. 11, the value of the cost $Q$ is decreased through the first 1000 iterations. Overall, we see that the proposed method is successful also for ROM-CL under the large time interval.



*Prepared using* acsauth.cls
DOI: 10.1002/acs

## 7. CONCLUSIONS AND FUTURE WORK

In this paper, we develop a learning-based robust observer design for POD-ROM models of the Boussinesq equations. We prove ISS between the states estimation error and the uncertain parameters estimation error. Then, we use ES for online estimation of model parametric uncertainties. The proposed method is applied to the 2-D Boussinesq equations, which illustrates the good performance in estimating the entire POD time coefficients, i.e., the entire profile of temperature and velocity which can be obtained by lifting the POD time coefficients to the $x$-domain by using the POD basis functions parametrization of the temperature and velocity. In future works, we will study the case of 3-D Boussinesq equations, which correspond to a more realistic model of indoor airflows related to practical applications in HVAC systems.

## REFERENCES

1. H. Khalil, *Nonlinear Systems*, 3rd ed. Prentice Hall, 2002.
2. M. Malisoff, F. Mazenc, Further remarks on strict input-to-state stable lyapunov functions for time-varying systems, *Automatica*, vol. 41, no. 11, pp. 1973 – 1978, 2005.
3. M. Arcak and P. Kokotovic, "Nonlinear observers: a circle criterion design and robustness analysis," *Automatica*, vol. 37, pp.1923-1930, 2001.
4. M. Benosman, J. Borgaard, O. San, and B. Kramer, "Learning-based robust stabilization for reduced-order models of 2D and 3D Boussinesq equations," *Applied Mathematical Modelling*, vol. 49, pp.162-181, 2017.
5. M. Benosman, *Learning-Based Adaptive Control: An Extremum Seeking Approach–Theory and Applications*. Butterworth-Heinemann, 2016.
6. J. Borgaard, J. A. Burns, A. Surana, and L. Zietsman, "Control, estimation and optimization of energy efficient buildings," In *2009 American Control Conference (ACC)*, pages 837–841. IEEE, 2009.
7. Z. Drmac and S. Gugercin, "A New Selection Operator for the Discrete Empirical Interpolation Method—Improved A Priori Error Bound and Extensions," *Methods and Algorithms for Scientific Computing*, vol. 32, num. 8, pp.631-648, 2016.
8. M.Chevalier, J. Hoepffner, T. R. Bewley, and D.S. Henningson, "State estimation in wall-bounded flow systems. Part 2. Turbulent flows," *Journal of Fluid Mechanics*, vol. 552, pp.167-187, 2006.
9. S. Dashkovskiy and A. Mironchenko, *Input-to-state stability of infinite-dimensional control systems*. Mathematics of Control, Signals, and Systems, 2013.
10. S. Dubljevic, N. H. El-Farra, P. Mhaskar, and P. D. Christofides, "Predictive control of parabolic PDEs with state and control constraints". *International Journal of Robust and Nonlinear Control: IFAC-Affiliated Journal*, vol. 16, no. 16, pp. 749-772, 2006.
11. M. Guay and N. Harihatan, "Airflow velocity estimation in building systems," In *2008 American Control Conference (ACC)*, pages 908–913. IEEE, 2009.
12. T. John, M. Guay, N. Hariharan, and S. Narayan, "POD-based observer for estimation in Navier–Stokes flow," *Computers & chemical engineering*, vol. 34.6, pp. 965–975, 2010.
13. V. L. Kalb, and A. E. Deane, "An intrinsic stabilization scheme for proper orthogonal decomposition based low-dimensional models," *Physics of fluids*, vol. 19.5, 054106, 2007.
14. M. Krstic, and H. H. Wang, "Stability of extremum seeking feedback for general nonlinear dynamic systems," *Automatica*, vol. 36.4, pp. 595–601, 2000.



*Prepared using* acsauth.cls
DOI: 10.1002/acs

15. W. MacKunis, S. V. Drakunov,M. Reyhanoglu, and L. Ukeiley, " Nonlinear estimation of fluid flow velocity fields," In *50th Conference on Decision and Control (CDC)*, pages 6931–6935, 2011.
16. E. D. Sontag, and Y. Wang, "New characterizations of input-to-state stability," *IEEE Transactions on Automatic Control*, vol. 41, pp. 1283-1294, 1996.
17. Y. Tan, D.R. Nesic, I.M. Mareels, and A. Astolfi, "On global extremum seeking in the presence of local extrema," *Automatica*, vol. 45, pp. 245–251, 2009.
18. R. Temam, and J. Tribbia, "Open boundary conditions for the primitive and Boussinesq equations," *Journal of the Atmospheric Sciences*, vol. 60.21, pp. 2647–2660, 2003.
19. O. San and J. Borggaard, "Principal interval decomposition framework for POD reduced-order modeling of convection Boussinesq flows," *International Journal for Numerical Methods in Fluids*, vol. 78, pp. 37–62, 2015.
20. S. Lele, Compact finite difference schemes with spectral-like resolution, *Journal of Computational Physics*, vol. 103, no. 1, pp. 16–42, 1992.
21. S. Gottlieb and C.-W. Shu , "Total variation diminishing RungeKutta schemes," *Mathematics of Computation*, vol 67, no 221, pp. 73?85, 1998.
22. Y. Wang and J. Zhang , "Sixth order compact scheme combined with multigrid method and extrapolation technique for 2D Poisson equation," *Journal of Computational Physics*, vol 228, no 1, pp. 137-146, 2009.
23. X. Xu, B. Huang, and S. Dubljevic, "Optimal continuous-time state estimation for linear finite and infinite-dimensional chemical process systems with state constraints," *Journal of Process Control*, vol. 35, pp. 127-142, 2015.
24. M. Benosman and J. Borggaard, "Robust nonlinear state estimation for a class of infinite-dimensional systems using reduced-order models," *International Journal of Control*, pp.1-12 , 2019.
25. Holmes, P., Lumley, J.L., and Berkooz, G. (1998), *Turbulence, coherent structures, dynamical systems and symmetry*, Cambridge University Press.
26. L. Wang, S. Chen, and K. Ma., "On stability and application of extremum seeking control without steady-state oscillation," *Automatica*, vol. 68, pp. 18–26, 2016.
27. M. Benosman, A-M. Farahmand, M. Xia, "Learning-based iterative modular adaptive control for nonlinear systems," *Int J Adapt Control Signal Process*, vol. 33, pp. 335– 355, 2019.




DOI: 10.1002/acs

## APPENDIX A DESIGN OF THE OBSERVER GAIN $L$ VIA LMI

For a system

$$\dot{x}(t) = Ax + Bu, \tag{84}$$

$$y = Cx, \tag{85}$$

We design the observer

$$\dot{\hat{x}}(t) = A\hat{x}(t) + Bu + L(y - C\hat{x}(t)). \tag{86}$$

The error system is

$$\dot{\tilde{x}}(t) = (A - LC)\tilde{x}(t). \tag{87}$$

We design the observer gain $L$ so that there exists a positive matrix $P$ which satisfies the following Lyapunov equation

$$P(A - LC) + (A - LC)^T P < 0, \tag{88}$$

which is equivalent to (through the expansion),

$$A^T P + PA - C^T L^T P - PLC < 0. \tag{89}$$

Since $L$ and $P$ are unkown variables, $PL$ is a nonlinear term on the unknown variables. Hence, we define $M := -PL$. Then, the matrix inequality becomes

$$A^T P + PA + C^T M^T + MC < 0, \tag{90}$$

under the constraint $P > 0$. Now, the problem is to find $P$ and $M$ such that the linear matrix inequality (90) holds. By Schur's compliment, the problem is equivalent to the following matrix inequality

$$\begin{bmatrix} A^T P + PA + C^T M^T + MC & 0 \\ 0 & -P \end{bmatrix} < 0, \tag{91}$$

which can be solved by LMI solver in MATLAB.




DOI: 10.1002/acs